JOURNAL OF OPTOELECTRONICS AND ADVANCED MATERIALS Vol. 10, No. 8, August 2008, p. 1984 - 1987

Diagnosis and dynamics of low energy electron beams using DIADYN

S. MARGHITU*, C. OPROIU[a], D. TOADER[a], C. RUSET[a], E. GRIGORE[a], O. MARGHITU[b], M. VASILIU[c]
ICPE Electrostatica, Bucharest, Romania
[a]*National Institute for Lasers Plasma and Radiation Physics, Bucharest, Romania*
[b]*Institute for Space Sciences, Bucharest, Romania*
[c]*POLITEHNICA University of Bucharest, Bucharest, Romania*

The paper presents original results concerning electron beam diagnosis and dynamics using DIADYN, a low energy (10–50 kV), medium intensity (0.1–1 A) laboratory equipment. A key stage in the operation of DIADYN is the beam diagnosis, performed by the non-destructive, modified three-gradient method (MTGM). We concentrate on the better use of experimental and computational techniques, in order to improve the consistency of the results. At present, DIADYN is equipped with a hot filament vacuum electron source (VES), consisting of a convergent Pierce diode, working in a pulse mode. Since the plasma electron sources (PES) have a longer lifetime and produce higher beam currents, we discuss the possibility to replace the VES with a PES. Special attention is given to VES results in a functioning regime typical for a low energy glow discharge PES.

(Received March 1, 2008; accepted June 30, 2008)

Keywords: Emittance, Space-charge, Beam diganosis, Beam dynamics, Gas discharge plasma sources

1. Introduction

Our previous investigations [1, 2] were focused on the non-destructive beam diagnosis at the source exit and on the beam dynamics in the transport channel. In a low energy beam channel with axial symmetry, consisting of magnetic lenses and free spaces, the root-mean-square (rms) beam radius, R, is governed by the equation [3, 4].

$$\frac{d^2R}{dz^2}+\frac{\eta B^2}{8U}R=\underbrace{\frac{1}{4\pi\varepsilon_0\sqrt{2\eta}}\frac{I}{U^{3/2}}\frac{1}{R}}_{T_{spch}}+\underbrace{\frac{\varepsilon^2}{R^3}}_{T_{em}} \qquad (1)$$

where I = beam current, U = beam acceleration potential, ε = rms beam emittance, B = axial magnetic field, η = electron charge-to-mass ratio, ε_0 = dielectric constant, *Tspch* = space-charge term, and *Tem* = emittance term. For low energy medium current electron beams (LEMCEBs, cf. [1]), used e.g. in material science applications, *Tspch* ≈ *Tem*, and both terms have to be taken into account when solving Eq. (1).

As indicated by recent LEMCEB results, in order to have adequate control of the experiments one needs: (a) a good knowledge of the beam parameters, (b) a well designed electron beam channel (EBC), and (c) a fair understanding of the beam dynamics.

In using DIADYN we have concentrated so far on the conditions (a) and (c). We developed the Modified Three Gradient Method, MTGM [1], for the non-destructive beam diagnosis, and investigated several beam regimes, by numerical simulations and experimental cross-checks.

Work presented in [2] emphasized the importance of condition (b) and made clear that DIADYN needs hardware adjustments of the EBC. These adjustments, in the meanwhile implemented, [5], help preventing the current loss between the electron source and the beam profile monitors, as well as observing the paraxial approximation implied by Eq. (1).

2. Experimental setup

The DIADYN installation consists of: (a) the beam system, (b) the vacuum system, including a mechanical and a diffusion pump, (c) a high voltage pulse generator, (d) a two-channel oscilloscope, and (e) data acquisition and data processing PCs. The beam system is presented in Fig. 1. The beam energy, *eUi*, is determined by the high voltage, *Ui*, applied to the source anode. The beam current at the source exit, *Ia*, depends both on *Ui* and on the heating voltage, *Ufil*, of the cathode filament. *Ui* is measured with the high-voltage probe HVP (see Fig. 1), while *Ia* is collected on a Faraday cage. Several regimes of the VES, *Ia=Ia(Ui, Ufil)*, are shown in Fig. 2, where the functioning point used later in this paper is indicated by a red circle.

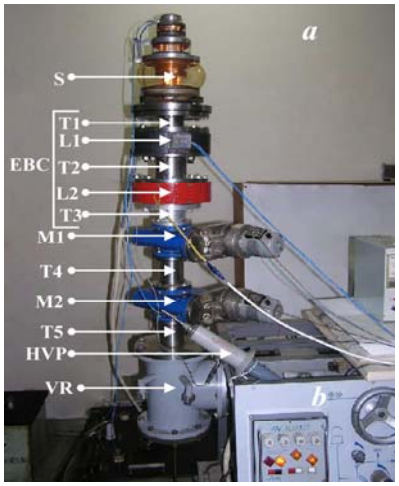

*Fig. 1. DIADYN beam system (a), and part of the vacuum system, (b). The beam system consists of: (i) a pulsed Pierce diode electron source, **S**, providing 4 μs beams, at 100 Hz, with Ia and Ui in the ranges 0.05–1A and 10–50keV; (ii) the electron beam channel, **EBC**, made up of the magnetic lenses **L1**, **L2**, and the field free spaces **T1**–**T5**; (iii) the vacuum room, **VR**; (iv) a beam monitoring unit, including two beam profile monitors **M1**, **M2**, the high-voltage probe **HVP,** and a sliding Faraday cage (not visible). The profile monitors consist of thin (0.25 mm), thermally resistant wires that scan the beam back and forth at constant speed.*

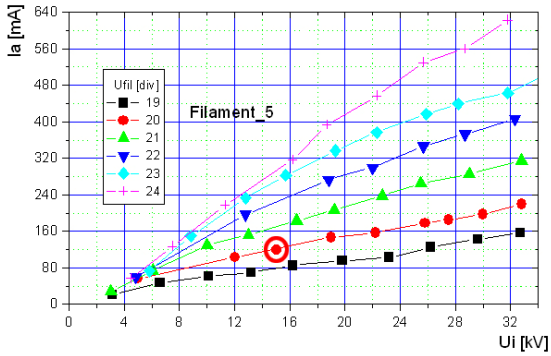

Fig. 2. Functioning points of the DIADYN source. The point used in the paper is indicated by the red circle, Ia=120 mA, Ui=15 kV, Ufil=20 div.

3. Non-destructive diagnosis with MTGM

After selecting the functioning point, the beam parameters (ε, R_o, z_o) are determined by the MTGM, with R_o and z_o the radius and position of the object cross-over. A proper measurement of the beam radius by M1 and M2, as function of the L1 lens power, $RMex = f(U_{L1})$, is essential for the success of the MTGM. For each lens power the beam profile at the two monitors is read on the oscilloscope. The beam crossing duration and the known scanning velocity of the profile monitor provide the beam radius. A dedicated fit program uses $RMex = f(U_{L1})$ and Eq. (1) to find the beam parameters. Recently, the MTGM was improved in two ways:

- The beam parameters provided by MTGM are quite sensitive to the beam radius estimates. The evaluation of the beam radius from the oscillograms recorded for M1 and M2 is critical for the consistency of the results. The radius has to be measured in *rms* sense, at a certain fraction – that can vary with z – of the pulse height, *h*.
- The fit program used by the MTGM was improved, by replacing the Monte-Carlo core of the code with a steepest descent minimization, based on the Powell algorithm [6]. The upgraded program is much faster, the solution is more stable, and the parameter set is derived with better accuracy.

In Fig. 3 we compare experimental and simulated results, where the simulations are based on beam parameters inferred from M1 data. The functioning point is *Ia* = 120 mA, *Ui*=15 kV, *Ufil*=20 div (see Fig. 2), and the derived beam parameters are ε = 92.6 mm mrad, R_0 = 3.9 mm, z_0 = –134.9 mm. The experimental beam radii, *RM1ex*, fed into the MTGM are measured by M1 at 0.2 h. The computed data, *RM1c* and *RM2c*, are obtained by integrating Eq. [1] with the parameters inferred above, R_0 and z_0 providing the initial conditions.

For the time being, the beam radius is estimated manually, from the recorded oscillograms, which leads to a certain error in the beam parameters. As seen in Fig. 3, the practical implications of this error are negligible for M1 (as expected, since the beam parameters are based on M1 data), but significant for M2. The disagreements at M2 might be related to the location of the image cross-over, close to or in front of M2 (see the discussion in the next section).

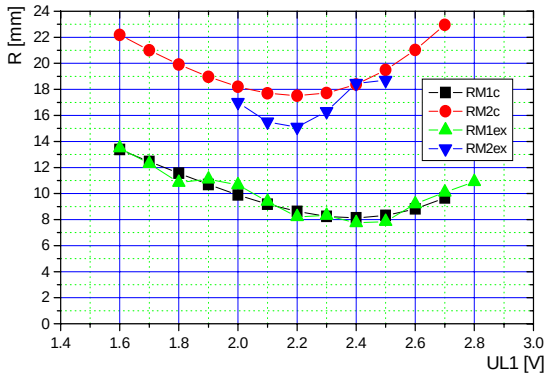

Fig. 3. Measured (RM1ex, RM2ex) and computed (RM1c, RM2c) beam radii. The measured radii depend on UL1, the voltage applied to the lens L1, and are estimated at 0.2 h. The computed radii are derived by integrating Eq. (1), with rms emittance, ε, and initial conditions, (z_0, R_0), inferred, via MTGM, from the M1 data. In this case ε = 92.6 mm mrad, R_0= 3.9 mm, z_0= –134.9 mm.

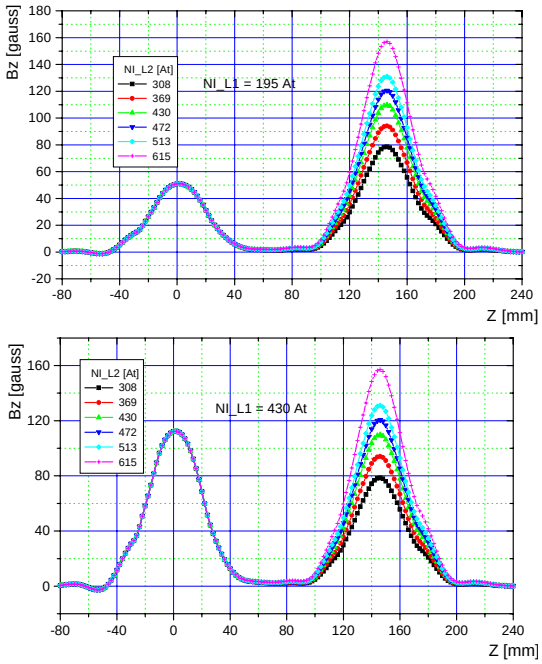

Fig. 4. Axial magnetic field for the beam dynamics experiments illustrated in Fig. 5. The magnetic field in the two panels is quite different at the lens L1 (maximum values of 52 gauss in the top panel and 113 gauss in the bottom panel), but similar at the lens L2, used for fine tuning.

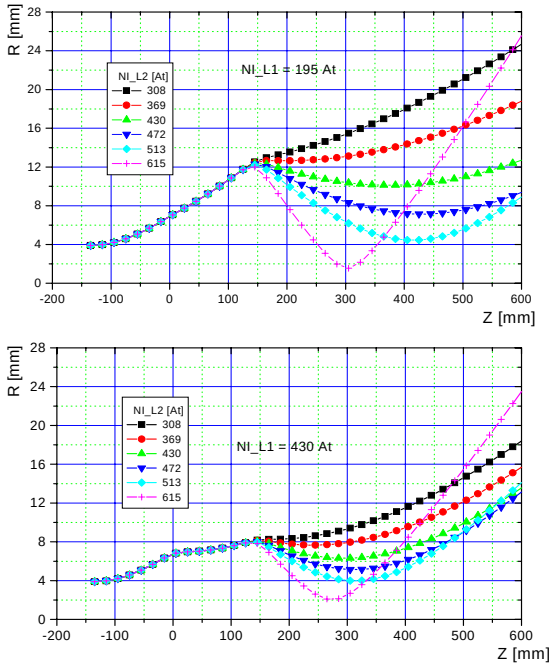

Fig. 5. Beam dynamics for the 12 EBC regimes indicated in Fig. 4. One notes the fine tuning role of L2 at moderate NI_L2. At high L2 powers, L1 has little influence on the radius but makes a significant difference in the position of the image cross-over.

4. Beam dynamics in a PES regime

Once the beam diagnosis is completed, the derived parameters are used further to determine the beam dynamics, and ultimately to control the beam cross-section in the target plane. A key element for a successful application is the electron beam channel (EBC), which for DIADYN includes two magnetic lenses and a number of field free spaces (see Fig. 1). With two magnetic lenses it is possible to vary at the same time both the position and the radius of the image cross-over, which provides the flexibility needed in applications. One can bring the image cross-over in the target plane, for an optimum power transfer, and at the same time adjust the image cross-over radius, in order to obtain the required power density level.

As already mentioned in the Introduction, in order to prevent the current loss and fulfil the paraxial approximation, implied by Eq. (1), the magnetic lenses have to be carefully designed and executed [5]. To achieve this goal we used a finite element code [7], and cross-checked the simulated axial magnetic field with the measured field. The agreement was quite good, of the order of 1%, which is the required level of magnetic field accuracy [8].

Since our plan is to replace the VES of DIADYN with a low energy glow discharge PES, in the following we shall present and discuss results obtained for the regime introduced in the diagnosis section, namely Ui=15 kV, $Ufil$=20 div, Ia=120 mA, ε=92.6 mm mrad, R_0=3.9 mm, z_0 = –134.9 mm. Although Ui can be lower and Ia higher for a low energy glow discharge PES, this regime provides a reasonable approximation of the PES conditions.

With the parameters above, we integrated Eq. (1) and obtained estimates of the beam radius at M1 and M2. We checked the evolution of the beam rms envelope for 12 different regimes of the EBC, shown in Fig. 4. In 6 of these regimes the L1 current (and power) is low, NI_L1 = 195 At (top panel), while for the other 6 regimes the L1 current is moderate, NI_L1 = 430 At (bottom panel). For each case we explored 6 L2 currents (and associated powers), NI_L2 = 308, 369, 430, 472, 513, 615 At.

The corresponding beam envelopes are presented in Fig. 5. It is clear that, by varying the power of both L1 and L2, one can control both the location and the radius of the image cross-over, with L2 serving for fine tuning. As long as NI_L2 is not too high, its gradual increase results in a gradual shift to the right, up to a maximum z, of the image cross-over, and a gradual decrease in its radius. If NI_L2 increases further, the cross-over location moves quickly back to lower z and, as discussed below, the computed beam evolution becomes often less reliable. In this *cross-over return region* the power density of the beam maximizes, and the changes in NI_L1 result in changes of the cross-over location, at roughly equal radius. This regime, potentially important for applications, requires further examination.

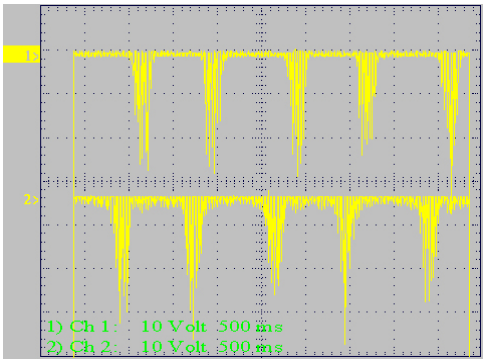

Fig. 6. Beam cross-sections at M1 (top) and M2 (bottom) as recorded on the oscilloscope.

Table 1. Experimental and computed beam radii at M1 and M2, corresponding to Fig. 5.

	NI_L1 = 195 At, Fig. 5 top					
NI_L2 [At]	**308**	**369**	**430**	**472**	**513**	**615**
RM1ex / RM1c [mm]	15.3/ 15.5	12.4/ 13.1	9.1/ 10.4	7.8/ 8.3	5.7/ 6.2	10.9/ 1.5
RM2ex/ RM2c	18.1/ 21.2	11.6/ 16.3	11.1/ 11.0	8.1/ 7.6	- / 5.7	- / 16.6
	NI_L1 = 430 At, Fig. 5 bottom					
NI_L2 [At]	**308**	**369**	**430**	**472**	**513**	**615**
RM1ex / RM1c [mm]	8.9/ 9.4	7.8/ 8.0	6.9/ 6.3	5.7/ 5.2	7.1/ 4.0	10.2/ 2.7
RM2ex / RM2c [mm]	14.9/ 14.8	15.8/ 12.3	18.5/ 10.1	- / 9.2	- / 9.3	- / 15.8

The computed estimates of the beam radius at M1 (z = 300 mm) and M2 (z = 500 mm), for the 12 EBC regimes, were compared with experimental measurements. Figure 6 shows an example of experimental raw data, for NI_L1=195 At and NI_L2=430 At. The complete set of computed versus measured radii is given in Table 1.

At low L1 power, NI_L1=195 At, the agreement is quite good for M1, except for NI_L2=615 At, where the cross-over has returned to M1. For M2 the agreement is good only at NI_L2 = 430 and 472 At, less good when NI_L2 is low, and poor when NI_L2 is high. With low NI_L2 the calculated cross-over is virtual, unlike the experimental cross-over which is real. With high NI_L2 the cross-over is in front of M2 and in the return region. Here the beam radius is too large to be measured with reasonable accuracy.

At moderate L2 power, NI_L1=430 At, there is good agreement for M1 up to NI_L2=472 At. For the two highest NI_L2 values, where the cross-over is in the return region and close to or in front of M1, the agreement is poor. For M2 we have good agreement only at low NI_L2, below 369 At, when both the calculated and the experimental cross-overs are virtual. At higher NI_L2 there is a real cross-over in front of M2, and the agreement becomes poor.

We suspect that the disagreements between computed and measured beam radii can be traced back to violations of the paraxial approximation. Additional effort is required to clarify the two types of disagreement identified above: *(i)* virtual calculated versus real experimental cross-over, and *(ii)* cross-over located in front of the target (and, often, also in the return region).

5. Conclusions

The laboratory installation DIADYN offers good conditions for experiments on low energy electron beams, with substantial potential for practical applications. Recent adjustments of the hardware and refinements of the software have improved the reliability of the beam diagnosis and the predictability of the beam dynamics, which are pre-requisites for the practical use of the beam.

Table 1 summarizes the results obtained with a vacuum electron source in a functioning regime typical for a plasma electron source. It shows that we have a good control of the beam dynamics as long as the target plane is in front of the image cross-over. Considering the rather extended range of target plane locations and beam radii / power densities consistent with this condition, the work so far provides a promising basis for the planed use of DIADYN with a plasma source.

For a complete control of the beam evolution more work is needed to understand the disagreement between the computed and measured beam radii when the image cross-over is in front of the target plane. Together with a closer examination of the cross-over return region, this may lead to a substantial gain in the efficiency of the beam use.

References

[1] S. Marghitu**,** O. Marghitu, C. Oproiu, G. Marin, Fl. Scarlat, Nucl. Instr. Meth. **B 217**, 498 (2004).
[2] S. Marghitu, O. Marghitu, M. Rizea, C. Oproiu, M. Vasiliu, Proc. 8th Int. Conf. on Electron Beam Technologies, Varna, Bulgaria, in Elektrotehnika i Elektronika, E + E, Nr. 5-6, 276 – 280, 2006.
[3] I. M. Kapchinskij and V.V. Vladimirskij, Proc. Int. Conf. High En. Accel., CERN, 274 - 288, 1959.
[4] P.Ciuti, Nucl. Instr. Meth., 93, 295-299, 1971.
[5] S. Marghitu, C. Matei, C. Oproiu, O. Marghitu, D. Toader, Analele Universităţii de Vest, Timişoara, Seria Fizică, 49, 97 – 101, 2007.
[6] W. Press, S. Teukolsky, W. Vetterling, B. Flannery, *Numerical recipes in C*, Chapter 10, Cambridge Univ. Press, 1997.
[7] M. Rizea, Rom. J. Phys., 37, 1031 – 1051, 1992.
[8] S. Marghitu, D. Martin, C. Oproiu, O. Marghitu, R. Cramariuc, Nucl. Instr. Meth. B, 113, 114–118, 1996.

*Corresponding author: silviamarghitu@yahoo.com